



**HAL**  
open science

## On the Reliability of Inverse Optimal Control

Jessica Colombel, David Daney, François Charpillet

► **To cite this version:**

Jessica Colombel, David Daney, François Charpillet. On the Reliability of Inverse Optimal Control. 2022 International Conference on Robotics and Automation (ICRA), May 2022, Philadelphia, United States. pp.8504-8510. hal-03349528v1

**HAL Id: hal-03349528**

**<https://inria.hal.science/hal-03349528v1>**

Submitted on 20 Sep 2021 (v1), last revised 5 Sep 2022 (v2)

**HAL** is a multi-disciplinary open access archive for the deposit and dissemination of scientific research documents, whether they are published or not. The documents may come from teaching and research institutions in France or abroad, or from public or private research centers.

L'archive ouverte pluridisciplinaire **HAL**, est destinée au dépôt et à la diffusion de documents scientifiques de niveau recherche, publiés ou non, émanant des établissements d'enseignement et de recherche français ou étrangers, des laboratoires publics ou privés.

# On the Reliability of Inverse Optimal Control

Jessica Colombel, David Daney, and François Charpillat

**Abstract**—Inverse Optimal Control is popular to analyze human motion. However, in the context of these methods it is necessary to better pay attention to the reliability of the results. This paper proposes an approach based on the evaluation of Karush-Kuhn-Tucker conditions relying on a complete analysis with Singular Value Decomposition. With respect to a ground truth, our simulations illustrate how the proposed analysis guarantees the reliability of the resolution. After introducing a clear methodology, the properties of the matrices are studied with different noise levels and different experimental model and conditions. We show how to implement the method step by step by explaining the numerical difficulties encountered during the resolution and thus how to make the results of the IOC problem reliable

Human Motion Analysis, Identification, Inverse Optimal Control.

## I. INTRODUCTION

Human motion analysis is relevant to provide a robot response adapted to human behavior. It is important to understand how this biological motion is generated and what are the elements that impact it, whether they are external factors such as the task to be performed or internal factors such as emotions [1]. Many methods have been developed to try to understand these different factors, such as Fourier methods [2], PCA [3], as well machine learning [4]. One interesting method focuses on the analysis of motion, hypothesizing that its generation can be considered an optimal problem.

The Inverse Optimal Control (IOC), similar to Inverse Reinforcement Learning [5], for human motion analysis is based on the assumption that human motion is a trajectory resulting from an optimisation process in which a given set of cost functions is minimized (or in case of Reinforcement Learning a given set of Reward function is maximized). The goal is then to find the associated cost functions. In addition to better understand the control that governs human movement [6], IOC is used in robotics in two main areas. First, reproduction of human-like motion for robotics [7], [8], especially for humanoids. Second, for human-robot interaction as prediction [9], [10] or as a way of understanding the division of task [11]. Human locomotion is one of the most studied motions [12]–[15] as well as its style [16]. A recent paper also explores affect in arm motion [17]. These publications underlined that behavior change can be studied with this method.

Two main approaches are used to solve the IOC problem. The first one is called Bi-Level and relies on the convergence of sequential Direct Optimal Control (DOC) towards the reference trajectories [7], [14], [18]. The issue with this approach is the time and computing cost. The second approach, named Approximate Inverse Optimal Control (AIOC), is

based on the necessity of respecting the optimality conditions provided by Karush-Kuhn-Tucker (KKT) [19] which are interpreted as a residual minimization process [20], [21]. This method allows to decrease the computational cost compared to the Bi-level methods which enable to process, inline, a trajectory through a sliding window. However, the resulting cost function can be far away from the reality if a rigorous mathematical analysis of the problem is not done.

This paper proposes to revisit the AIOC problem through an analysis with Singular Values Decomposition of matrices associated with linear systems figuring the KKT optimality conditions.

The main contributions of the paper are : (i) details of the properties of the methods that provide indices to the feasibility and identifiability of the parameters; (ii) analysis of the reliability approach regards to measurement noise. The results are presented on a simple simulation of a 2-bar robotic arm. This allows the robustness results to be highlighted with knowledge of the original state.

First, this paper introduces the IOC method and the proposed resolution, then it details the analysis and interpretation of the problem. The experiment in simulation are provided before presenting the results and the discussion.

## II. INVERSE OPTIMAL CONTROL METHOD

### A. Direct Optimal Control formulation

A strong hypothesis considers that human motion trajectories (noted  $\mathbf{s}$ ) is generated by optimizing of a convex criterion  $C(\mathbf{s})$ , under  $n_f$  constraints  $f_i(\mathbf{s})$  ( $i = 1, \dots, n_f$ ) that allows to model it as a Direct Optimal Control problem as follows:

$$\mathbf{s} = \arg \min C(\mathbf{s}) \text{ s.t. } f_{1, \dots, n_f}(\mathbf{s}) = 0 \quad (1)$$

where  $\mathbf{s} \in \mathbb{R}^{n_s \times n_t}$  is a trajectory composed, by  $n_t$  of frames ; each are defined by a state  $\mathbf{x}_t$  of dimension  $n_s$ , such that  $\mathbf{s} = [\mathbf{x}_1, \dots, \mathbf{x}_t, \dots, \mathbf{x}_{n_t}]^T$ . In this paper, the states is given by  $\mathbf{x}_t = [x_t, \dot{x}_t, \ddot{x}_t]^T$  and  $f$  is the set of  $n_f$  equality constraints. Inequality constraints can also be considered, as in [22], but not presented in this paper for the sake of simplicity. Equality constraints  $f$  are defined by  $g$  that connect the variables and their derivative to figure the kinematics of the system, in addition to constraints on given values of the initial ( $\mathbf{x}_{start}$ ) and final ( $\mathbf{x}_{goal}$ ) states .

$$f : g(\mathbf{x}_1, \dots, \mathbf{x}_{n_t}) = 0 ; \mathbf{x}_1 - \mathbf{x}_{start} = 0 ; \mathbf{x}_{n_t} - \mathbf{x}_{goal} = 0 \quad (2)$$

Let  $C$  is the cost function to be minimized, their physical meaning will be given in the next section:

$$C(\mathbf{s}) = \sum_{k=1}^{n_c} \omega_k \sum_{t=1}^{n_s n_t} C_k(\mathbf{x}_t) \quad (3)$$

with  $\omega_k$  the  $k^{th}$  component of the weight normalized vector  $\boldsymbol{\omega}$  associated to the cost function  $C_k$ . To guarantee the convexity of this problem, it can be chosen that  $\omega_k \geq 0$  and  $C_k$  is quadratic for all  $k \in [1, n_c]$ .

### B. Cost functions for human motion

One of the issue to identify human motion is to model the motor control that the human will optimised to generate its motion. In the case of IOC, it means to select several cost functions which should be based on this motor behaviour. In the litterature, there are two main approaches to define these cost functions. The first one is to consider the kinematic of the motion, for example, the jerk to report its smoothness [23]. Then the cost functions are build on kinematic criterion such as: the distance to goal, the velocity, the acceleration and, obviously the jerk. The second one is to explain the motion through torque-change in joints, then dynamics cost functions should be defined using energy, torque, angular power, e.g. [24].

IOC's literature studies human motion with all cost functions that can explain the motion either they are kinematics or dynamics and depending on the motion, different cost functions are highlighted. Moreover, descriptors for motion can qualify separately the task realized but also the style of the motion and it is possible to implement descriptors as cost functions to better describe the motion [25]. Recent paper shows these other types of cost functions as Laban's effort (time, space, etc.) or quantity of motions to explore the affect part of a motion [17].

### C. Inverse Optimal Control through KKT formulation

The goal of inverse optimal control is to find those objective functions weights  $\omega_k$  from a given trajectory  $\mathbf{s}^*$  supposed to be optimal, knowing the cost functions  $C_k$  for all  $k = 1, \dots, n_c$  and equality constraints  $f_i$  for all  $i = 1, \dots, n_f$ .

One approach is based on Karush-Kuhn-Tucker optimality conditions. Let  $\mathbf{s}^*$  be an optimal trajectory associated with  $\boldsymbol{\omega}$ . First, defining the Lagrangian  $L$  associated to the direct optimisation problem of equation 1 :

$$L(\mathbf{s}^*, \boldsymbol{\lambda}) = \sum_{k=1}^{n_c} \omega_k C_k(\mathbf{s}^*) + \sum_{i=1}^{n_f} \lambda_i f_i(\mathbf{s}^*) \quad (4)$$

with  $\boldsymbol{\lambda} \in \mathbb{R}^{n_f}$  is the vector of  $n_f$  Lagrange multiplier  $\lambda_i$  of equality constraints functions  $f$ .

Let's the observed state vector  $\mathbf{s}^*$  be considered as the optimal trajectory associated with  $\boldsymbol{\lambda}$ . Therefore, to minimize the Lagrangian  $L$ , its derivative  $\frac{\partial L}{\partial \mathbf{s}}(\mathbf{s}^*)$ , evaluated at  $\mathbf{s}^*$ , must be equal to the vector zero.

$$\frac{\partial L}{\partial \mathbf{s}}(\mathbf{s}^*, \boldsymbol{\lambda}) = \sum_{k=1}^{n_c} \omega_k \frac{\partial C_k}{\partial \mathbf{s}}(\mathbf{s}^*) + \sum_{i=1}^{n_f} \lambda_i \frac{\partial f_i}{\partial \mathbf{s}}(\mathbf{s}^*) = \mathbf{0} \quad (5)$$

Moreover, as  $\mathbf{s}^*$  is computed according to the constraints describes in Equation 1, we get:

$$f_i(\mathbf{s}^*) = 0, i = 1, \dots, n_f \quad (6)$$

These two lasts equations 5 (stationary condition) and 6 (primal feasibility condition) are included in KKT conditions. Solving the inverse optimal control problem corresponds to identify the unknown vector weight ( $\boldsymbol{\omega}$  as well as the associated Lagrange multiplier  $\boldsymbol{\lambda}$ ) subject to these conditions.

### D. Resolution using KKT conditions

The equation 5 can be rewritten as  $\mathbf{J} \cdot \mathbf{z} = \mathbf{0}$  with:

$$\underbrace{[\mathbf{J}_\omega, \mathbf{J}_\lambda]}_{\mathbf{J}} \cdot \underbrace{\begin{pmatrix} \boldsymbol{\omega} \\ \boldsymbol{\lambda} \end{pmatrix}}_{\mathbf{z}} = \mathbf{0} \quad (7)$$

and

$$\mathbf{J}_\omega = \left[ \frac{\partial C_1}{\partial \mathbf{s}}(\mathbf{s}) \dots \frac{\partial C_{n_c}}{\partial \mathbf{s}}(\mathbf{s}) \right], \mathbf{J}_\lambda = \left[ \frac{\partial f_1}{\partial \mathbf{s}}(\mathbf{s}) \dots \frac{\partial f_{n_f}}{\partial \mathbf{s}}(\mathbf{s}) \right]$$

Classically, we remark that:

- If  $\mathbf{J}$  is not singular the equation 7 admit only the trivial solution  $\mathbf{z} = \mathbf{0}$ . This means that the trajectory  $\mathbf{s}^*$  does not correspond to any trajectory minimizing the criterion  $C(\mathbf{s})$  (equation 3) and this whatever the value of  $\boldsymbol{\omega}$ .
- If  $\mathbf{J}$  is singular, this means that  $\mathbf{z}$  is a vector of the null-space of  $\mathbf{J}$ .

In the last case,  $\mathbf{z}$  can be easily obtained thought the Singular Value Decomposition of  $\mathbf{J}$  such that  $\mathbf{U}\mathbf{S}\mathbf{V}^T = \mathbf{J}$  with  $\sigma_1, \dots, \sigma_L$  the singular values ordered descending, given by the diagonal of  $\mathbf{S}$ ,  $V_1, \dots, V_L$  the right singular vector associated with  $\sigma_1, \dots, \sigma_L$  such that the orthogonal matrix  $\mathbf{V}^T = [V_1^T, \dots, V_L^T]^T$  and  $\mathbf{U}$  also a orthogonal matrix. Then, if rank deficiency of  $\mathbf{J}$  is equal to 1 ( $\sigma_L = 0$ ), the solution for  $\mathbf{z}$  is  $V_L$ .

If  $\mathbf{z} = V_L$  then

$$\underbrace{\mathbf{U} \cdot \mathbf{S} \cdot \mathbf{V}^T}_{\mathbf{J}} \cdot \mathbf{z} = \mathbf{U} \cdot \mathbf{S} \cdot \begin{pmatrix} V_1^T \cdot V_L \\ \vdots \\ V_L^T \cdot V_L \end{pmatrix} = \mathbf{U} \cdot \begin{pmatrix} 0 \\ \vdots \\ 0 \\ \sigma_L \end{pmatrix} \quad (8)$$

and  $\|\mathbf{J} \cdot \mathbf{z}\| = \sigma_L$

Note that a re-normalization of  $\mathbf{z} = V_L$  is necessary to provide values to  $\boldsymbol{\omega}$  such that  $\boldsymbol{\omega} = (V_{L1}, \dots, V_{Ln_c})^T / \|(V_{L1}, \dots, V_{Ln_c})^T\|$ .

If more that one singular values are equal to zero, each linear combinations of singular vector associated to null singular values can be a solution of  $\mathbf{z}$  for equation 7. However, the physical interpretation of this case is problematic and will be discussed in section II-F.

In an ideal case, the resolution of Equation 7 solves the IOC problem. However, in real applications, trajectories and models suffer from inaccuracies making the IOC problem more complex to solve, e.g  $\sigma_L$  should not be equal to zero but near to zero. This is why, according to equation 8 we propose to use the lower singular value as an indicator of the quality of the approximation of  $\mathbf{z}$  by  $V_L$ . Our challenge is to analyse the reliability of the IOC solutions. Given that the singular values are not zero, to what extent can we trust the

recovered vector? This paper shows that the singular values are indices of the reliability of the solution to this problem.

### E. Difference with AIOC approach

Our previous proposal insists on the solving of equation 5 and reformulated in equation 7. However, previous section shows that the uncertainties prevent us from obtaining a clear solution and this will be discussed in the next section.

Classically, this problem is considered by the community by transforming the solving problem, given in equation 5 into a constrained minimization problem by considering the residuals  $r_s(\omega, \lambda, s) = \mathbf{J}(s) \cdot [\omega, \lambda]^T$ . The stationary condition is then called stationary residuals  $r_s$  and the aim of the method is to find the minimum of its square norm in  $(\omega, \lambda)$  as :

$$\begin{aligned} \underset{\omega, \lambda}{\text{minimize}} \quad & \|r_s(\omega, \lambda, s)\|^2 \\ \text{s.t.} \quad & \omega_k \geq 0, k = 1, \dots, n_c. \end{aligned}$$

The additional constraints ( $\omega_k \geq 0$ ) ensure the convexity of the criterion used in the COD (see end of the section II-A). There are several methods to solve this problem as a Quadratic Programming algorithm. However, this formulation of the problem admits drawback. It always provides a solution whatever the nature on the real optimality of the considered trajectory ( $s = s^*$ ) with respect to the  $\omega$  solution. Moreover, the inequality constraints project the values on positive without control of the approximation made. Thus, it becomes difficult to rely on the solution found. This paper presents an analysis of reliability of the IOC problem based on Singular Values study.

### F. Rank analysis and reliability

As mentioned in section II-D, the ideal case is rank-deficient of 1 for  $\mathbf{J}$ , meaning that an optimal trajectory exists in the set defined by constraints  $f$  in regards to the criterion  $C(s)$ .

In the opposite case, several cases can be explained :

- **Identifiability of  $\omega$  or  $\lambda$**  With regards of the equation 5, it is not possible to identify  $\omega$  (resp.  $\lambda$ ) if the rank of  $\mathbf{J}_\omega$  (resp.  $\mathbf{J}_\lambda$ ) is not equal to  $\dim \omega$  (resp.  $\dim \lambda$ ). This case is very classical in parameter's identification and needs to be checked. It can be done by a QR decomposition of  $\mathbf{J}_\omega$  (or  $\mathbf{J}_\lambda$ ) to detect and compute the dependencies between parameters  $\omega$  (or  $\lambda$ ), see [26].

In the case of rank deficiency of  $\mathbf{J}_\omega$ , this phenomenon can have several origins. First, the cost functions  $C_k$  are linearly dependants generating a redundant information on the cost of the trajectories. This dependencies can be formal, due to a bad definition or selection of the basis  $C$  or punctually numerical for a particular trajectory  $s$ . Another case can happen if a basis is not dependent to trajectory's parameters. The weak identifiability is a complex case which appears when one (or several) of the bases of  $C$  is not very excited by the evaluated trajectory. In these conditions the value of the smallest

singular value of  $\mathbf{J}_\omega$  is low but not null: in this case, a selection criterion, often associated by a normalization of the matrix  $\mathbf{J}_\omega$ , is needed to exclude properly the base(s): some strategies can be implemented as [27] for a calibration problem.

The rank deficiency of  $\mathbf{J}_\lambda$  is linked to a bad parametrization of the manifold described by  $f$ , i.e. the number of constraints is not minimal to represent the set of trajectories. This introduces additional  $\lambda$  not necessary.

In both case ( $\mathbf{J}_\omega$  and  $\mathbf{J}_\lambda$ ), the full identifiability of  $\omega$  and  $\lambda$  have to be verified before process to an IOC resolution process, this to prevent (in part) the rank-deficient of  $J$  greater than 1.

- **Full rank of  $\mathbf{J}$  (but not near singular)** In this case, the equation 5 do not admit a solution (except the trivial solution  $z=0$ ). The tested trajectory is not optimal regard to  $C(s)$  whatever the choice of  $\omega$ . In this case, we prefer not to provide a solution to the IOC problem because its reliability is questionable.
- **$\mathbf{J}$  is near singular** Because of the uncertainties related to the observation of the trajectory in real conditions, it is difficult to determine if the matrix  $\mathbf{J}$  is quiet singular or not. However, we propose a decision criterion which is one contribution of this paper. The quantification of singular values is problematic because the numerical zero is dependent on the floating-point relative accuracy and the size of the matrices. Moreover, we need to integrate the tolerance allowed between the observed trajectory and the trajectory reconstructed from the result of the IOC ( $\omega_k$ ). However, this approach is incompatible with the online calculation requirements. In this paper, the evaluation of the drop in between singular values is used instead of pure rank as a good criteria to interpret the problem and the results. A simple algorithm to detect the drop is used. Additionally, the normalization of the matrices allows to amplify the difference between the singular values clarifying the criterion on the rank. Under these conditions, if a drop in the singular values is detected, we consider the matrix as singular.
  - If this drop is equal to 1, the solution of  $z$  is the lower right singular vector  $\mathbf{V}_L$ . The weights  $\omega_k$  are then deduced if and only if their values are positive in order to certify that the criterion  $C(s)$  is convex; otherwise we prefer, again, not to provide a solution.
  - If this drop is greater than 1 and the identifiability of  $\omega$  and  $\lambda$  have been verified ( $\mathbf{J}_\omega$  and  $\mathbf{J}_\lambda$  are full rank), every linear combinations of the singular vectors associated to the singular values considered as null is a solution for  $z$ . Thus the IOC problem would have multiple solutions with a dimension equal to the rank fall. We believe that this case is due to the approximation of the rank under specific conditions and that only the lower null singular value is significant. An example will be given in section IV but the question remains open. However, this example also shows the danger of using

the stationary residue minimization approach.

### III. EXPERIMENT SIMULATIONS

#### A. Simulation

The first example proposed is a two-links robot arm. It is defined by  $\mathbf{s}_t = [\theta_{1,t}, \theta_{2,t}, \dot{\theta}_{1,t}, \dot{\theta}_{2,t}, \ddot{\theta}_{1,t}, \ddot{\theta}_{2,t}]^T$  the state of the two-link robot arm with  $\mathbf{s} = [\mathbf{s}_1, \dots, \mathbf{s}_{n_t}]^T$  the trajectory of the system to go from a start point 1 ( $\mathbf{s}_{start}$ ) to an objective point  $n_t$  ( $\mathbf{s}_{goal}$ ). The dynamics of the two-link robot arm is expressed as followed:

$$\boldsymbol{\tau}_t = \mathbf{M}(\boldsymbol{\theta}_t) \cdot \ddot{\boldsymbol{\theta}}_t + \mathbf{R}(\boldsymbol{\theta}_t, \dot{\boldsymbol{\theta}}_t) \dot{\boldsymbol{\theta}}_t + \mathbf{g}(\boldsymbol{\theta}_t) \quad (9)$$

with  $\boldsymbol{\tau}_t = [\tau_1, \tau_2]^T$  the torques applied to each joint,  $\mathbf{M}$  the positive-definite inertia matrix,  $\mathbf{R}$  the Coriolis matrix and  $\mathbf{g}$  the gravity vector. All the equations detailing this model will be in appendix I.

The cost functions of the 10 trajectories of simulation are presented with their cost weight in Table I with  $C_k = \{\tau_1^2, \tau_2^2, \ddot{\theta}_1^2, \ddot{\theta}_2^2, \dot{\theta}_1^2, \dot{\theta}_2^2, (\dot{\theta}_1 \tau_1)^2, (\dot{\theta}_2 \tau_2)^2\}$ . The equality constraints  $f$  are defined by:

$$\mathbf{f}(\mathbf{s}) \begin{cases} \mathbf{s}_1 - \mathbf{s}_{start} \\ \mathbf{s}_{n_t} - \mathbf{s}_{goal} \\ \forall i \in [1, n_t - 1] \\ \begin{bmatrix} \theta_{i+1} \\ \dot{\theta}_{i+1} \end{bmatrix} - \begin{bmatrix} \theta_i \\ \dot{\theta}_i \end{bmatrix} - \Delta t \begin{bmatrix} \dot{\theta}_i \\ \ddot{\theta}_i \end{bmatrix} \end{cases} = \begin{pmatrix} 0 \\ \vdots \\ 0 \end{pmatrix}_{(2n_s + n_t(n_s - 2)) \times 1}$$

with the same values for each trajectories  $\mathbf{s}_{start} = [0, 0, 0, 0, 0, 0]$  and  $\mathbf{s}_{goal} = [\pi/2, \pi/2, 0, 0, 0, 0]$ .

Remark: The simulations are done with Matlab R2019a. The DOC is done with *fmincon*. The matrix  $\mathbf{J}$  is chosen to be normalised with a norm 1 which corresponds to the maximum absolute column sum of the matrix. It was found more robust than other types of norms for the examples proposed (2, infinit and forbenius, as in [11]). The normalisation of  $\boldsymbol{\omega}$  is done with norm 2.

The simulation steps are as follows:

- 1) Generate a reference trajectory with DOC and  $\boldsymbol{\omega} = \boldsymbol{\omega}_{ref}$  for each trajectory of the Table I as presented in section II-A;
- 2) Modification of the basis (III-B) or addition of measurement noise (III-C);
- 3) Resolution of IOC as presented in section II-D to obtain  $\boldsymbol{\omega}_{sol}$ ;
- 4) Generate new trajectories with DOC from the found vector weight  $\boldsymbol{\omega}_{sol}$ ;
- 5) Analysis of the results (III-D), by comparing previous trajectories with reference ones.

#### B. Identification of basis

A preliminary question is to define by hypothesis the cost functions that could have been used to generate the human movement, its state variables and the associated constraints. For human movement it is all the more difficult as we do not really know what cost functions are associated with each

type of movement. This section tests different types of trials to simulate a number of problems or errors that can affect the IOC implementation. They correspond to case described in section II-F :

- Cost function symbolically correlated among all the cost functions proposed;
- One cost function missing among those used to generate the motion;
- Cost functions added with no linked with the initial ones, in the results it is called "useless functions".

#### C. Noise level

This paper proposes to explore the effects of noise uncertainties on the reliability of the results. Uncertainties is designed as white Gaussian noise with mean  $m = 0$  and different values of the variance  $var$ . Two types of noise will be tested. The first test it what is called "constant noise": the same noise level will be applied to all observed states (i.e. angle, velocity and acceleration). This test makes it possible to investigate the violation of the problem's equality constraints. The second test, called "real noise" is only added once on angles. Other state variables are obtained by derivation without additional noise. This is designed to simulate the kind of data that can be retrieved in real life using simple sensors. In addition, it allows the constraints to be maintained but the cost functions are more impacted. For both tests, the ten trajectories are being assessed for 8 noise level with  $var$  from  $10^{-7}$  to  $10^0$  with 10 repetitions of each with randomize noise.

#### D. Evaluation criteria

To compute the error between  $\boldsymbol{\omega}_{ref}$  used to generate the reference trajectory by a COD and the one identified by IOC  $\boldsymbol{\omega}_{sol}$  presented in Section II-D the dot product is assessed. It gives the similarity to  $\boldsymbol{\omega}_{ref}$ . It is important to notice that all  $\boldsymbol{\omega}$  are normalized and that all  $\omega_k$ 's have the same sign (necessary condition for convexity,  $\boldsymbol{\omega} \geq \mathbf{0}$  to within one sign). In addition to the comparison of  $\boldsymbol{\omega}$ , the Root Mean Square Error (RMSE) between the initial trajectory and the trajectory generate with the  $\boldsymbol{\omega}$  found by AIOC is assessed to evaluate the precision of the algorithm. The trajectory means here the state vector composed of angular position, velocity and acceleration. Finally, the rank drop by singular values are assessed.

## IV. RESULTS

#### A. Identification of basis

The different tests on the identification of basis are computed on all the trajectories and the resulting RMSE are assessed. The results are presented in Table II. The first line of this table presented the results in ideal case. The average and standard deviation of RMSE is  $3.3E^{-5} \pm 5.0E^{-5}$ . With the adding of 6 "useless" cost functions, the RMSE is almost equal to the one in ideal case with a mean of  $3.6E^{-5}$  and standard deviation of  $3.8E^{-5}$ . For both ideal case and useless cost functions, the mean of the rank drop of  $\mathbf{J}_{\boldsymbol{\omega}}$  is of  $1.1 \pm 0.32$ . It is not of mean 1 because trajectory 5 has

with our algorithm a rank of 2 even though  $\mathbf{J}_\omega$  and  $\mathbf{J}_\lambda$  are full rank. However the other clue of reliability is  $\mathbf{w} \geq 0$  and in this case the  $\mathbf{w}$  does not meet this criterion.

As presented in part II-F, the number of correlated functions is linked with the fall in rank of  $\mathbf{J}$  but especially of  $\mathbf{J}_\omega$ . The rank drop of  $\mathbf{J}_\omega$  is of 1 for all trajectories, while the mean of  $\mathbf{J}$  is  $1.8 \pm 0.42$ . Once the QR algorithm is used and pinpointed the collinear functions, the fall in rank return to a fall of one and the proposed approach is able to determine good  $\omega$ . Without the QR algorithm, the average RMSE is of  $1.4E^2 \pm 2.2$ .

While one cost function is missing, the RMSE increases to  $2.8E^{51} \pm 8.9E^{51}$  with complete rank for  $\mathbf{J}$  (rank drop of  $0.1 \pm 0.32$ ) and  $\mathbf{J}_\omega$ .

It should be noted that the rank of  $\mathbf{J}_\lambda$  is always full with the same minimum ratio (0.26). Indeed, this submatrix is constant for the examples provided.

### B. Noise level

a) *Constant Noise:* All trajectories indicate an inflection point at which the noise is so high that the evolution of RMSE is erratic and it exceeds  $10^4$ . Before this point, the trajectories show a correlation between increased noise and increased RMSE on the reconstructed trajectory. For the trajectories 6 and 8 the inflection point is at a noise of  $10^{-3}$ . The trajectory 1 has its inflection point at a noise of  $10^{-1}$ . All the other trajectories have an inflection point at a noise of  $10^{-2}$ . After these points, the rank is systematically considered as full and  $\omega$  is irretrievable. For half of the trajectories this inflection point also corresponds to a change in the fall in rank. The trajectories still have a rank drop of 1 at this point, then it becomes full rank beyond. The other half is divided into two categories. The first, which includes trajectories 1 and 3, goes into full rank at the inflection point, but they exceed the RMSE error of  $10^{-1}$ . The second category includes trajectories 5, 6 and 7 which also pass

through the full rank before their inflection point but this does not correspond to high RMSE errors ( $\leq 10^{-1}$ ). Figure 1 show the example of three of the trajectories (1, 6, 9) to highlight these three types of behaviors and to explore the results in more detail. It is possible to see the evolution of the  $\omega_{sol}$  error in relation to the noise level. For trajectory 1, the similarity of  $\omega_{sol}$  to  $\omega_{ref}$  if of 1 until the noise level  $10^{-1}$  where it starts to decrease with 0.995. The trajectory 6 shows a decrease in similarity from 1 to 0.782 at  $10^{-3}$  which corresponds to a RMSE of  $6.9E^{-2}$ . Finally the trajectory 8 has an error in  $\omega_{sol}$  that decrease on the rank deficiency at the error level of  $10^{-2}$  (0.774385) before it increase again after on the two last noise levels (0.89794, 0.95311). These errors corresponds to a RMSE error on trajectory greater than  $10^{12}$ .

b) *Real Noise:* The results obtained with real noise are clear. Whatever the noise level, the RMSE quickly exceeds  $10^{10}$ . The most robust trajectories to this type of measurement noise are trajectories 1, 2, 9 and 10, whose RMSE is of the order of  $10^{-2}$  at a noise level of  $10^{-6}$  before exceeding  $10^4$  at a noise level of  $10^{-5}$ ; as well as trajectory 4, which even obtains a RMSE of  $4.9E^{-3}$  for a level noise of  $10^{-6}$ .

## V. DISCUSSION

### A. Identification of Basis

The results show that the ideal case does not generate the exact same trajectory with a RMSE of zero. This can be explain by the computing error and the precision of the arithmetic use. Therefore, all results should refer to this result for the ideal case. Then it is important to notice that the addition of cost functions hardly affects the results, provided that the added functions are not correlated. In contrast, if a function is missing, the trajectories are not recoverable.

Therefore, it is recommended to put as many cost functions as possible, paying attention to symbolic correlations.

	Torque		Jerk		Acceleration		Power	
	$\tau_1^2$	$\tau_2^2$	$\ddot{\theta}_1^2$	$\ddot{\theta}_2^2$	$\ddot{\theta}_1^2$	$\ddot{\theta}_2^2$	$(\dot{\theta}_1 \tau_1)^2$	$(\dot{\theta}_2 \tau_2)^2$
Traj 1	0.981	0.196	0	0	0	0	0	0
Traj 2	0.196	0.981	0	0	0	0	0	0
Traj 3	0.196	0.981	0.002	0.010	0	0	0	0
Traj 4	0.117	0.078	0	0	0.971	0.194	0	0
Traj 5	0.0002	0.001	0.002	0.010	0.981	0.196	0	0
Traj 6	0.004	0.004	0.007	0.007	0.707	0.707	0	0
Traj 7	0.019	0.097	0.002	0.010	0.971	0.194	0.019	0.097
Traj 8	0.096	0.172	0.010	0.002	0.957	0.191	0.019	0.096
Traj 9	0.019	0.097	0	0	0.971	0.194	0.097	0.019
Traj 10	0.019	0.097	0	0	0.971	0.194	0.019	0.097

TABLE I: Table of cost functions weight vector  $\omega$  for each trajectory generated in simulation. The cost functions are normalized.

	RMSE	$\omega$ error	$\mathbf{J}$ Rank drop	$\mathbf{J}_\omega$ Rank drop
Ideal Case	$3.3E^{-5} \pm 5.0E^{-5}$	$1 \pm 2.3E^{-9}$	$1.1 \pm 0.32$	$0 \pm 0$
Useless Functions	$3.6E^{-5} \pm 3.8E^{-5}$	$1 \pm 8.6E^{-6}$	$1.1 \pm 0.32$	$0 \pm 0$
Correlated function	$1.4E^2 \pm 2.2$	$0.15 \pm 0.27$	$1.8 \pm 0.42$	$1 \pm 0$
Function missing	$2.8E^{51} \pm 8.9E^{51}$	$0.78 \pm 0.33$	$0.1 \pm 0.32$	$0 \pm 0$

TABLE II: Table of results for tests on basis functions. The results are expressed as *mean  $\pm$  standard deviation* over the ten trajectories tested.

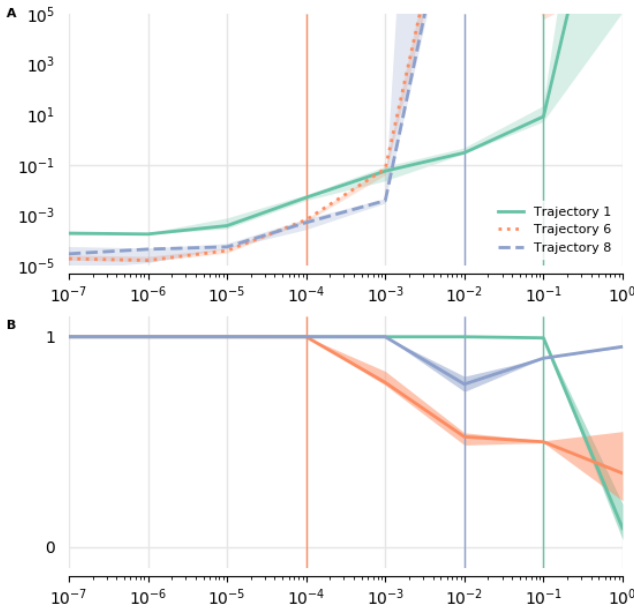


Fig. 1: This figure shows results on 3 trajectories for constant noise. Figure A illustrates the RMSE median and Figure B the median  $\omega$  error, in relation to the noise level. The shadows on both graph represent the percentile 25 and 75. The vertical coloured lines running through both graphs show the median of changes in rank, before the bar the rank deficiency is of 1, from the bar the rank is complete. No percentiles are illustrate for the change in rank because they are equal to the median.

Then it is essential to look at the ranks of the two sub-matrices to check that there is no identifiability problem. If the sub-matrix or sub-matrices are not of full rank, it is then possible to do a QR decomposition which will allow to find the superfluous column(s) of the sub-matrices.

Finally, even if the rank drop is of one, the last check is on  $\omega$ . If it does not meet the positivity condition, the result is automatically considered false. This may mean that one or more cost functions explaining the movement is missing.

### B. Noise Level

As the results show, the constant noise has much less impact than the real noise. This can be explained by the fact that successive first-order derivatives increase the noise on accelerations. This has a direct impact on the noise level on torques and jerks, for example. It is therefore very important to ensure measurement quality on the higher derivative variables. The types of sensors used in the experiments may influence the IOC results when analysing human movement. In addition, constant noise violates the KKT equalities constraints (Equation 6) but still allows information to be recovered up to a certain noise level. It can be deduced that it is more important to guarantee the quality of the cost functions variables than to maintain the constraints. Then, it is possible to use filters and polynomial functions to get as close as possible to the initial trajectories rather than trying

to maintain these constraints.

It is interesting to notice that the error on  $\omega$  does not indicates precisely the error the error made on the reconstructed trajectory. This is because the different cost functions do not impact the generation of the trajectory in the same way. Thus an error on  $\omega_k$ , does not impact the trajectory the same way if it is on  $\omega_{k+1}$ .

## VI. CONCLUSION

In this paper, an Inverse Optimal Control approach is proposed and discussed. It is shown that the singular values and the fall in rank can be good features to understand the reliability of the results obtained. The paper presents two different types of problematic with the interpretation of the results: the identifiability of the basis and the reliability under uncertainties. It is important to make sure that the model is well defined for cost functions and constraints. This information is studied independently in each matrix of the KKT stationary condition. It is recommended to use as many cost functions as possible, as long as the correlations between them are taken into account. The tests carried out on the robustness to noise indicate that the accuracy values associated to the variables present in the cost functions is not negligible. On the other hand, it is possible to violate the equality constraints of the model and still recover a reliable result. This reliability can be seen in the rank drop. The closer the last singular value is to the penultimate, the less reliable the results are. Thus, when the rank is full, there is a good chance that the trajectory is too noisy to recover the unknowns sought. The results proposed in this paper are intended to qualify the results obtained on real data.

## APPENDIX I

### DETAILED MODEL FOR SIMULATION

$$\mathbf{M}(\boldsymbol{\theta}) = \begin{bmatrix} a_1 + 2a_2\cos(\theta_2) & a_3 + a_2\cos(\theta_2) \\ a_3 + a_2\cos(\theta_2) & a_3 \end{bmatrix}$$

$$\mathbf{R}(\boldsymbol{\theta}, \dot{\boldsymbol{\theta}}) = \begin{bmatrix} -a_2\dot{\theta}_2\sin(\theta_2) & -a_2(\dot{\theta}_1 + \dot{\theta}_2)\sin(\theta_2) \\ a_2\dot{\theta}_1\sin(\theta_2) & 0 \end{bmatrix}$$

$$\mathbf{g}(\boldsymbol{\theta}) = \begin{bmatrix} b_1b_3\cos(\theta_1) + b_2b_3\cos(\theta_1 + \theta_2) \\ b_2b_3\cos(\theta_1 + \theta_2) \end{bmatrix}$$

$$a_1 = m_1r_1^2 + m_2(l_1^2 + r_2^2) + I_1 + I_2$$

$$a_2 = m_2l_1r_2$$

$$a_3 = m_2r_2^2 + I_2$$

$$b_1 = l_1m_2 + r_1m_1$$

$$b_2 = r_2m_2$$

$$b_3 = g = 9.81$$

and for each link :  $m_1 = 1, m_2 = 1.5\text{kg}$  are the mass,  $l_1 = 1, l_2 = 1.2\text{m}$  are the length,  $r_1 = 0.5, r_2 = 0.6\text{m}$  are the distance from the joint center to the center of mass and  $I_1 = 0.5, I_2 = 0.7\text{kgm}^2$

## REFERENCES

- [1] G. Venture, H. Kadone, T. Zhang, J. Grèzes, A. Berthoz, and H. Hicheur, "Recognizing Emotions Conveyed by Human Gait," *Int J of Soc Robotics*, vol. 6, no. 4, pp. 621–632, Nov. 2014.
- [2] C. Westhoff and N. F. Troje, "Kinematic cues for person identification from biological motion," *Perception & Psychophysics*, vol. 69, no. 2, pp. 241–253, Feb. 2007.
- [3] N. F. Troje, "Decomposing biological motion: A framework for analysis and synthesis of human gait patterns," *Journal of Vision*, vol. 2, no. 5, pp. 2–2, Sep. 2002.
- [4] T. Randhavane, U. Bhattacharya, K. Kapsaskis, K. Gray, A. Bera, and D. Manocha, "Identifying Emotions from Walking using Affective and Deep Features," *arXiv:1906.11884 [cs]*, Jun. 2019, arXiv: 1906.11884.
- [5] S. Albrecht, M. Ulbrich, and M. Leibold, "A bilevel optimization approach to obtain optimal cost functions for human arm movements," *NACO*, vol. 2, no. 1, pp. 105–127, Mar. 2012.
- [6] B. Berret, E. Chiovetto, F. Nori, and T. Pozzo, "Evidence for Composite Cost Functions in Arm Movement Planning: An Inverse Optimal Control Approach," *PLOS Computational Biology*, vol. 7, no. 10, p. e1002183, Oct. 2011.
- [7] K. Mombaur, A. Truong, and J.-P. Laumond, "From human to humanoid locomotion—an inverse optimal control approach," *Auton Robot*, vol. 28, no. 3, pp. 369–383, Apr. 2010.
- [8] T. Park and S. Levine, "Inverse Optimal Control for Humanoid Locomotion," p. 5.
- [9] J. Mainprice, R. Hayne, and D. Berenson, "Predicting human reaching motion in collaborative tasks using Inverse Optimal Control and iterative re-planning," in *2015 IEEE International Conference on Robotics and Automation (ICRA)*, May 2015, pp. 885–892.
- [10] S. Gaurav and B. Ziebart, "Discriminatively Learning Inverse Optimal Control Models for Predicting Human Intentions," in *Proceedings of the 18th International Conference on Autonomous Agents and Multi-Agent Systems*, ser. AAMAS '19. Montreal QC, Canada: International Foundation for Autonomous Agents and Multiagent Systems, May 2019, pp. 1368–1376.
- [11] W. Jin, D. Kulić, J. F.-S. Lin, S. Mou, and S. Hirche, "Inverse Optimal Control for Multiphase Cost Functions," *IEEE Transactions on Robotics*, vol. 35, no. 6, pp. 1387–1398, Dec. 2019.
- [12] D. Clever, K. Hatz, and K. Mombaur, "Studying Dynamical Principles of Human Locomotion using Inverse Optimal Control," *PAMM*, vol. 14, no. 1, pp. 801–802, 2014.
- [13] D. Clever, R. Malin Schemschat, M. L. Felis, and K. Mombaur, "Inverse optimal control based identification of optimality criteria in whole-body human walking on level ground," in *2016 6th IEEE International Conference on Biomedical Robotics and Biomechatronics (BioRob)*, Jun. 2016, pp. 1192–1199.
- [14] S. Albrecht, P. Basili, S. Glasauer, M. Leibold, and M. Ulbrich, "Modeling and Analysis of Human Navigation with Crossing Interferer Using Inverse Optimal Control," *IFAC Proceedings Volumes*, vol. 45, no. 2, pp. 475–480, Jan. 2012.
- [15] A.-S. Puydupin-Jamin, M. Johnson, and T. Bretl, "A convex approach to inverse optimal control and its application to modeling human locomotion," in *2012 IEEE International Conference on Robotics and Automation*, May 2012, pp. 531–536.
- [16] S. J. Lee and Z. Popović, "Learning behavior styles with inverse reinforcement learning," *ACM Trans. Graph.*, vol. 29, no. 4, pp. 122:1–122:7, Jul. 2010.
- [17] P. Carreno-Medrano, T. Harada, J. F.-S. Lin, D. Kulić, and G. Venture, "Analysis of Affective Human Motion During Functional Task Performance: An Inverse Optimal Control Approach," in *2019 IEEE-RAS 19th International Conference on Humanoid Robots (Humanoids)*, Oct. 2019, pp. 461–468.
- [18] P. Abbeel and A. Y. Ng, "Apprenticeship learning via inverse reinforcement learning," in *Proceedings of the twenty-first international conference on Machine learning*, ser. ICML '04. Banff, Alberta, Canada: Association for Computing Machinery, Jul. 2004, p. 1.
- [19] P. Englert, N. A. Vien, and M. Toussaint, "Inverse KKT: Learning cost functions of manipulation tasks from demonstrations," *The International Journal of Robotics Research*, vol. 36, no. 13-14, pp. 1474–1488, Dec. 2017.
- [20] A. Keshavarz, Y. Wang, and S. Boyd, "Imputing a convex objective function," in *2011 IEEE International Symposium on Intelligent Control*, Sep. 2011, pp. 613–619.
- [21] M. Johnson, N. Aghasadeghi, and T. Bretl, "Inverse optimal control for deterministic continuous-time nonlinear systems," in *52nd IEEE Conference on Decision and Control*, Dec. 2013, pp. 2906–2913.
- [22] A. Panchea, *Inverse optimal control for redundant systems of biological motion*. Orléans, Dec. 2015.
- [23] N. Hogan, "An organizing principle for a class of voluntary movements," *J Neurosci*, vol. 4, no. 11, pp. 2745–2754, Nov. 1984.
- [24] Y. Uno, M. Kawato, and R. Suzuki, "Formation and control of optimal trajectory in human multijoint arm movement," *Biol. Cybern.*, vol. 61, no. 2, pp. 89–101, Jun. 1989.
- [25] C. Larboulette and S. Gibet, "A Review of Computable Expressive Descriptors of Human Motion," in *Proceedings of the 2Nd International Workshop on Movement and Computing*, ser. MOCO '15. New York, NY, USA: ACM, 2015, pp. 21–28.
- [26] S. Besnard and W. Khalil, "Identifiable parameters for parallel robots kinematic calibration," in *Proceedings 2001 ICRA. IEEE International Conference on Robotics and Automation (Cat. No.01CH37164)*, vol. 3, 2001, pp. 2859–2866 vol.3.
- [27] T. Gayral and D. Daney, "A sufficient condition for parameter identifiability in robotic calibration," in *Computational Kinematics*. Springer, 2014, pp. 131–138.